

# Supporting Information

-

## In-vacuo XPS study: Controlled ALD growth of $\text{Al}_2\text{O}_3$ on metallic lithium enabled by plasma pretreatment

Tippi Verhelle,<sup>†</sup> Lowie Henderick,<sup>†</sup> Saeed Yari,<sup>‡,¶,§</sup> Siebe Coessens,<sup>†</sup> Matthias M.  
Minjauw,<sup>†</sup> Louis De Taeye,<sup>||</sup> Philippe M. Vereecken,<sup>||</sup> Jolien Dendooven,<sup>†</sup>  
Mohammadhosein Safari,<sup>‡,¶,§</sup> and Christophe Detavernier\*,<sup>†</sup>

<sup>†</sup>*Department of Solid State Sciences, Ghent University, Krijgslaan 285 S1, 9000 Gent,  
Belgium*

<sup>‡</sup>*Institute for Materials Research (IMO-imomec), UHasselt, Martelarenlaan 42, 3500,  
Hasselt, Belgium*

<sup>¶</sup>*Energyville, Thor Park 8320, 3600, Genk, Belgium*

<sup>§</sup>*imec Division IMOMEC, 3590, Diepenbeek, Belgium*

<sup>||</sup>*imec, Kapeldreef 75, Leuven, 3001, Belgium*

E-mail: Christophe.Detavernier@Ugent.be

## Starting surfaces

In order to obtain reproducible starting surfaces through plasma pretreatments, the pressure of the gas should be carefully controlled. Figure S1 shows the influence of plasma pressure on the removal of the native surface layer. For an Ar pressure of  $10^{-2}$  mbar, the native layer is barely removed, evident from the remaining carbonate peak at 293 eV. Only upon the use of lower pressures, ideally between  $1 \times 10^{-3}$  and  $< 5 \times 10^{-3}$  mbar, is the native oxide effectively removed and can the  $\text{Li}_2\text{O}$  surface be obtained in a reproducible manner. At lower pressures, the substrate surface is predominantly exposed to ion bombardment as the collision probability will be smaller.<sup>1</sup>

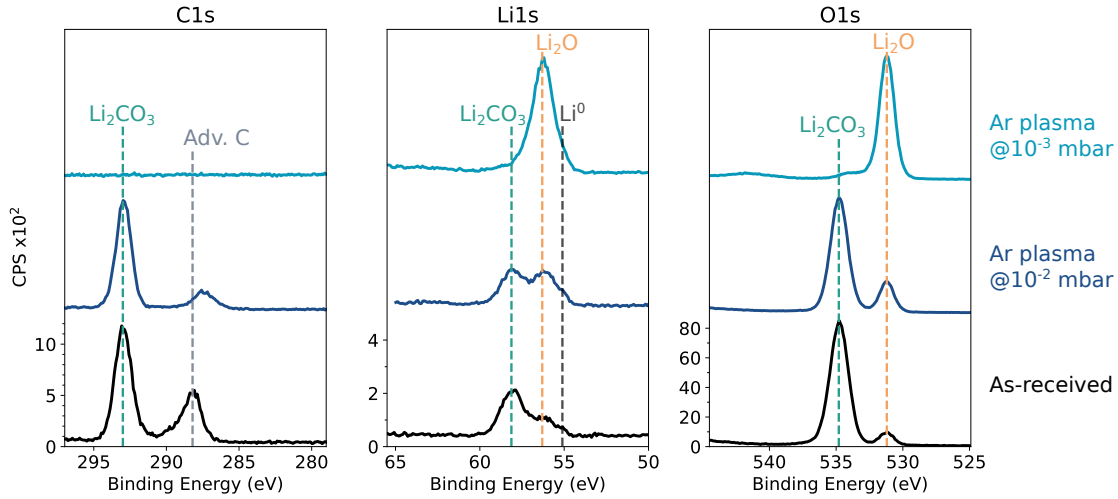


Figure S1: In-vacuo XPS of as-received and Ar plasma treated lithium foil with Ar pressure at  $10^{-2}$  and  $10^{-3}$  mbar at a substrate temperature of  $100^\circ\text{C}$ .

In Figure S2, surveys scans are shown for the initial starting surfaces discussed in Figure 2. In the case of  $O_2$  plasma, the C 1s signal is barely visible, meaning the small peak present in the high-resolution C 1s scan is negligible.

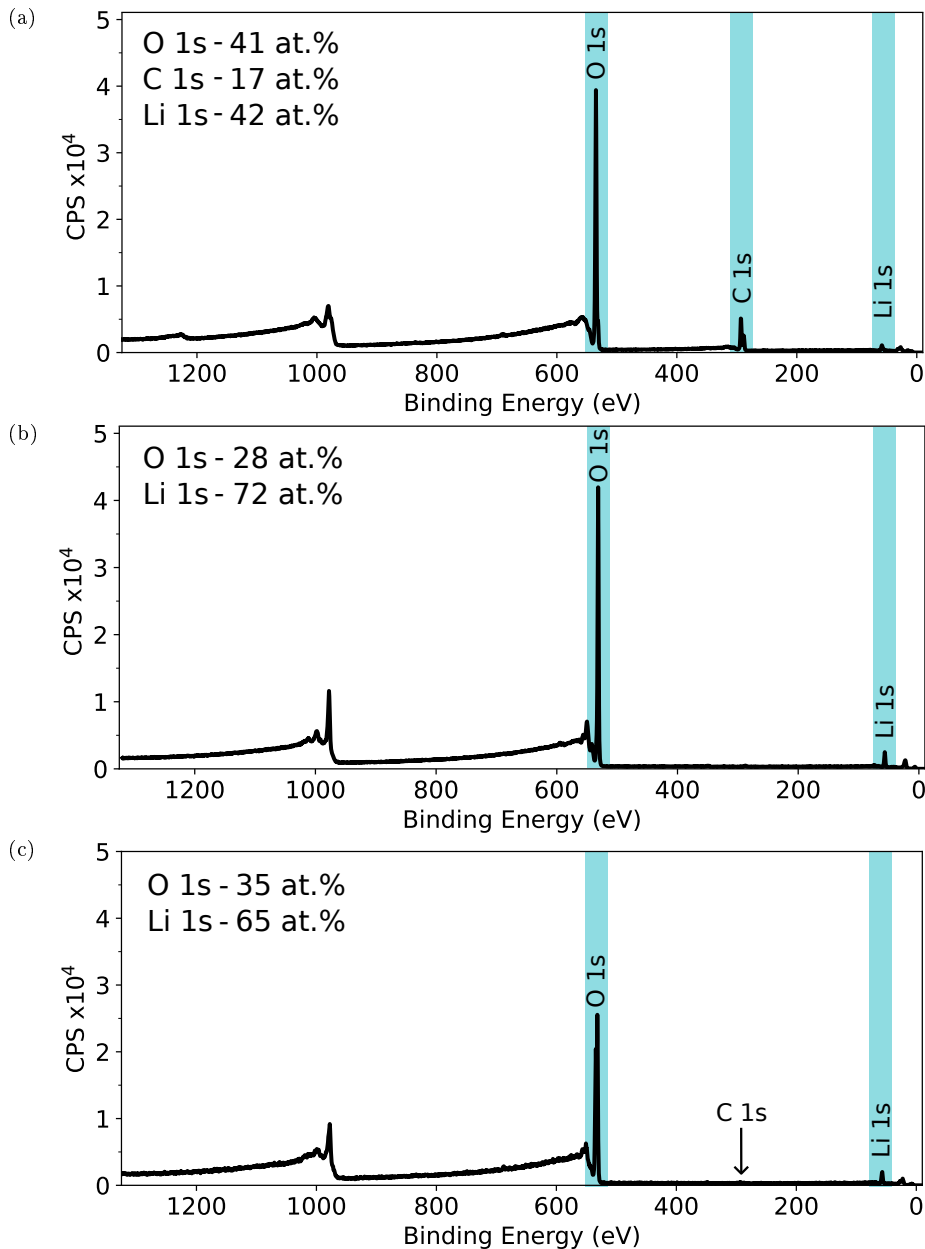


Figure S2: XPS survey scans of (a) as-received, (b)  $Ar^*$  pretreated and (c)  $O_2^*$  pretreated lithium foil.

With ARXPS, subsurface chemical states can be probed non-destructively within the XPS information depth. Figure S3 shows ARXPS measurements for as-received,  $Ar^*$  and  $O_2^*$  treated lithium foil at different emission angles. Smaller angles with respect to the surface

normal correspond to increased probing depth, while larger angles mean enhanced surface sensitivity. ARXPS amplifies the depth-dependent contrast, making the  $\text{Li}^0$  observable as a distinct shoulder.

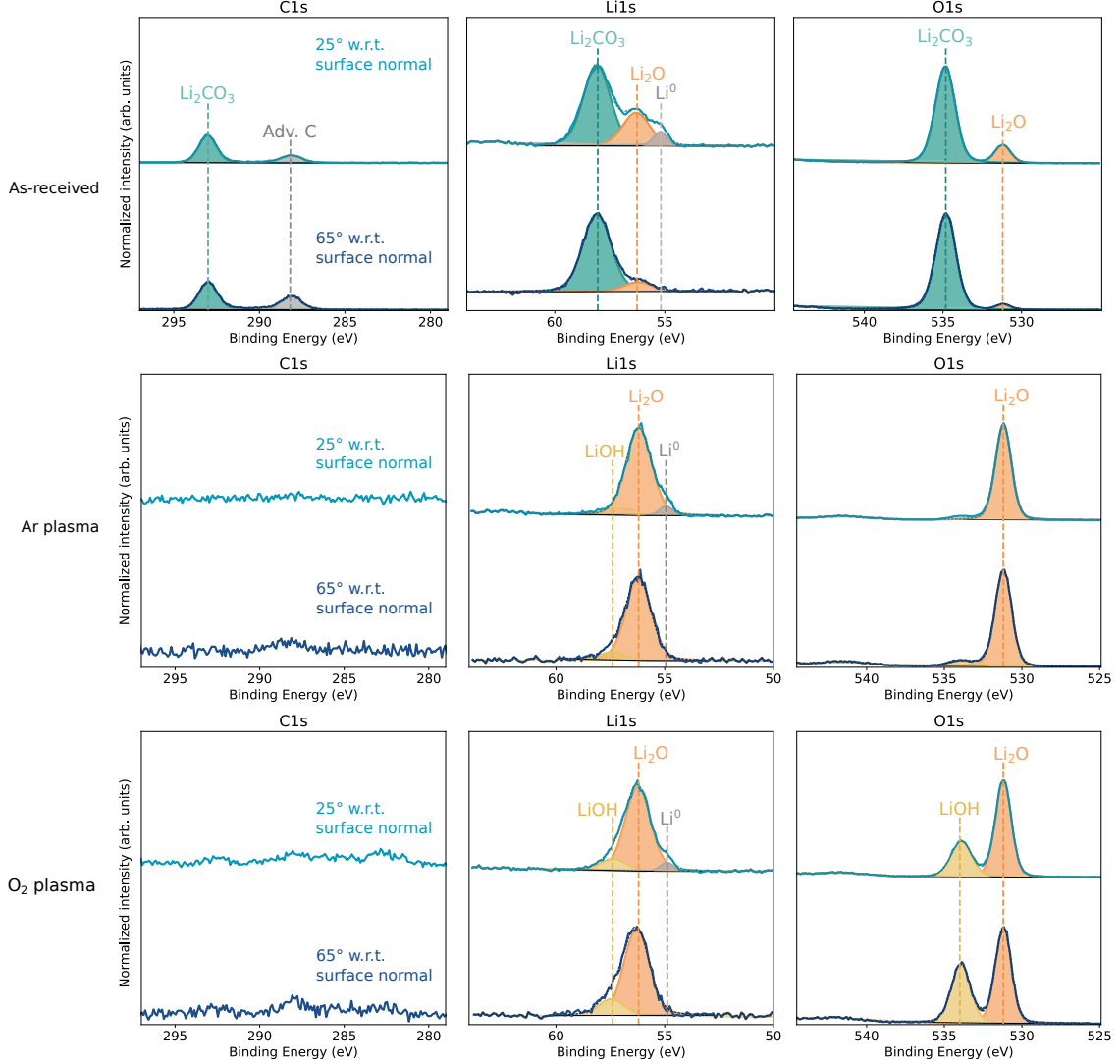


Figure S3: Angle-resolved XPS of as-received, Ar\* and O<sub>2</sub>\* treated lithium foil at emission angles of 25° and 65°.

## TMA exposure on as-received metallic lithium

After TMA exposure on as-received metallic lithium foil, large, dispersed nuclei were visible along the grain boundaries. EDX shows that these nuclei are decomposition products, as a lot of Al signal is detected. On smooth places without particles, a small amount of Al is detected, pointing at possible ALD-like reactions taking place at the same time as the TMA decomposition.

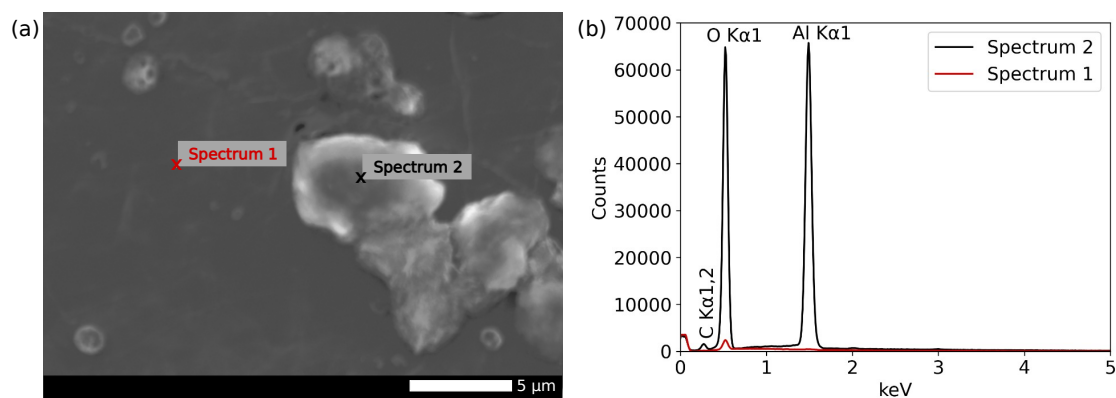


Figure S4: (a) SEM image and (b) EDX spectra of a nucleation particle (Spectrum 2) and its surrounding (Spectrum 1).

## TMA exposure on Ar plasma pretreated surface

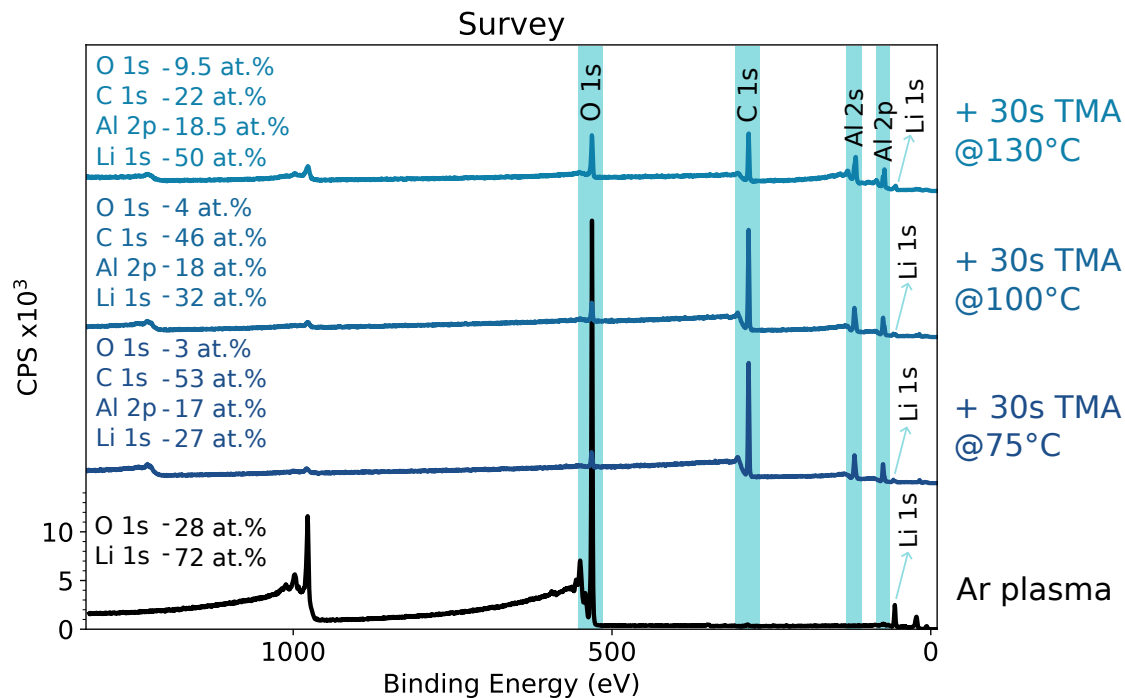


Figure S5: XPS survey scans of TMA exposure on Ar\* treated lithium foil at different substrate temperatures.

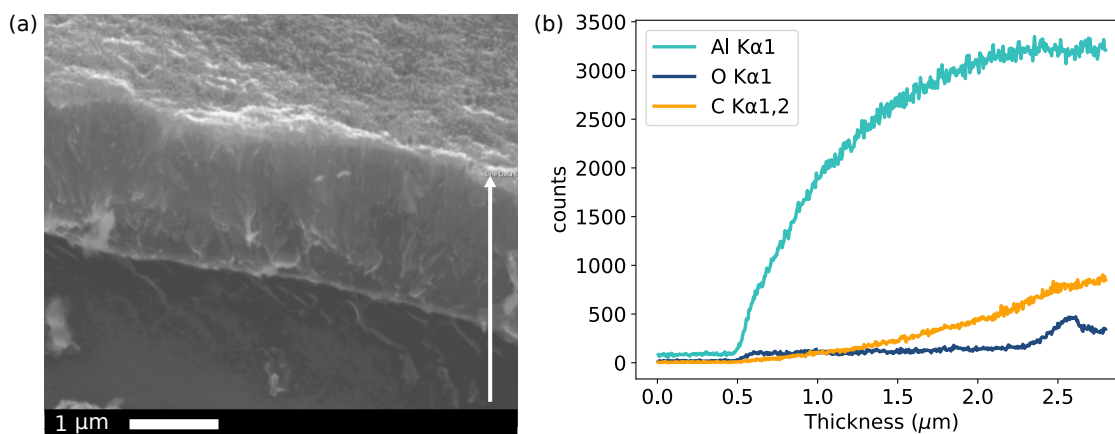


Figure S6: Ar plasma treated lithium foil exposed to 30s of TMA: (a) SEM cross-sectional image with the arrow indicating the direction of the linescan and (b) EDX linescan.

## TMA exposure on O<sub>2</sub> plasma pretreated surface

The saturation of TMA and O<sub>2</sub>\* on lithium during the first cycle was determined through XPS measurements by observing changes in the different spectra. Figure S7 shows high-resolution XPS scans for C 1s, Li 1s, O 1s and Al 2p, where the y-axes were kept the same to show real intensity differences.

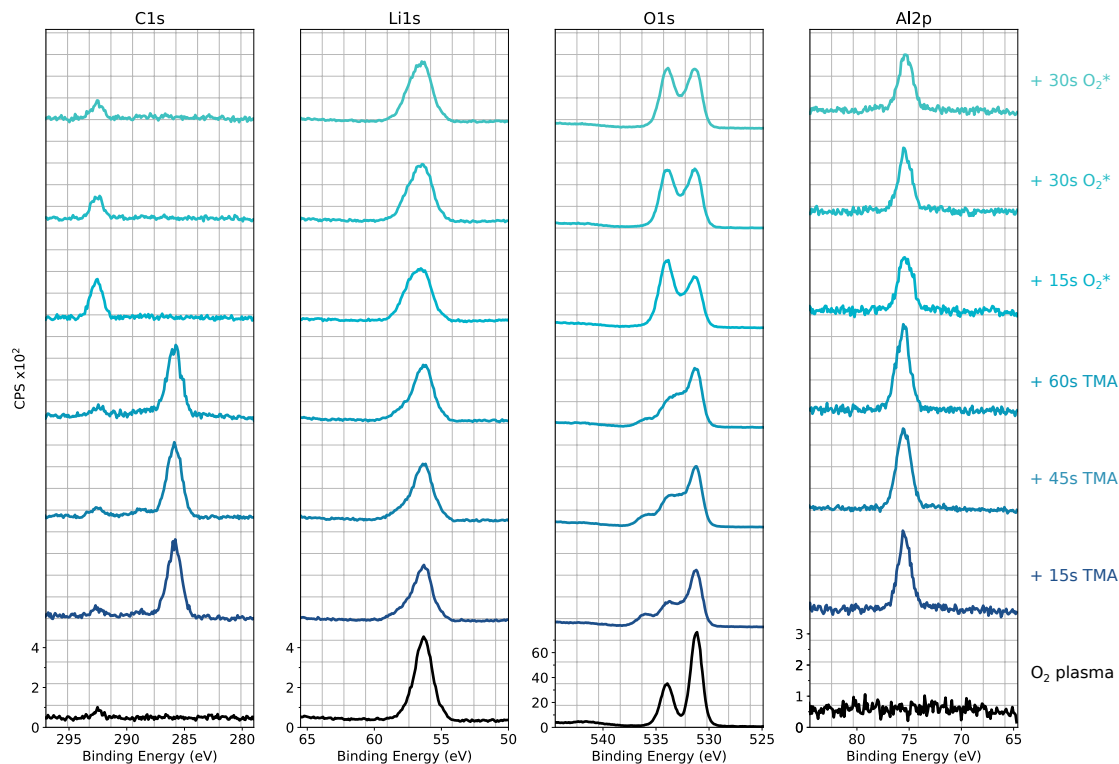


Figure S7: High-resolution XPS scans showing the saturation behavior of TMA and O<sub>2</sub>\* on an O<sub>2</sub>\* pretreated lithium foil.

Figure S8 shows survey scans for ALD of Al<sub>2</sub>O<sub>3</sub> on O<sub>2</sub>\* treated lithium. As discussed in Figure 7, a small peak is visible around 536 eV in the O 1s high-resolution scan. This peak only appeared after a TMA pulse. Simultaneously, visible from the survey spectra, a N 1s peak appears, hinting at contamination of NO<sub>x</sub> species. Where this contamination is coming from, is not obvious as it is not a typical contamination product of TMA, nor was a leak found in the TMA line.

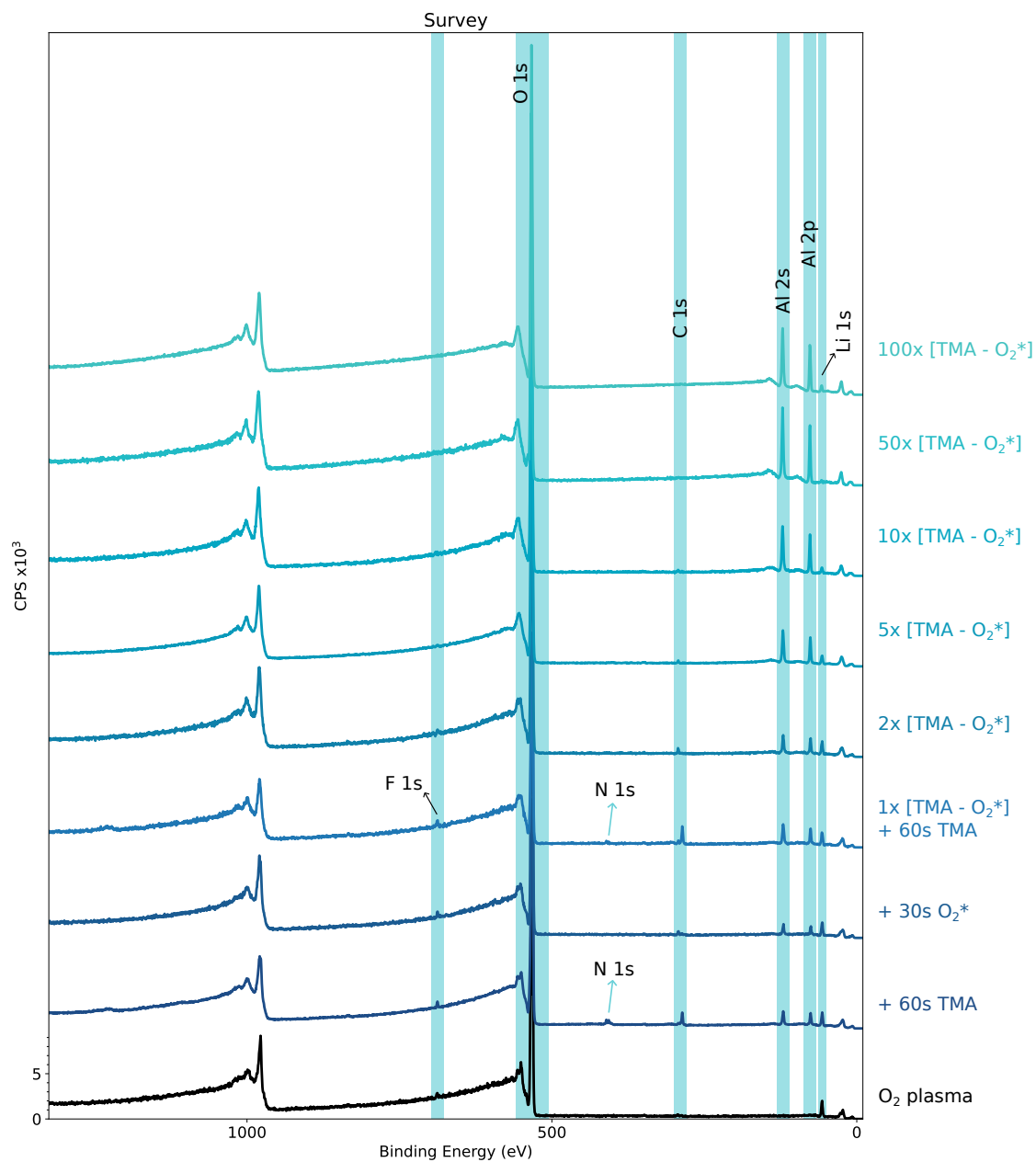


Figure S8: XPS survey scans of different ALD cycles on O<sub>2</sub>\* treated lithium foil.



Table 1: Atomic percentages of different ALD cycles on  $O_2^*$  treated lithium as determined by quantification of the survey spectra in Figure S8.

	O 1s (at.%)	C 1s (at.%)	Li 1s (at.%)	Al 2p (at.%)	N 1s (at.%)	F 1s (at.%)
$O_2$ plasma	34	1	65	-	-	-
+ 60s TMA	34.5	3	56	4.5	1.5	0.5
+ 30s $O_2^*$	33	1	62	4	-	-
1x [TMA - $O_2^*$ ] + 60s TMA	33	5	55	6	0.5	0.5
2x [TMA - $O_2^*$ ]	41	1	52	6	-	-
5x [TMA - $O_2^*$ ]	42	0.5	45.5	12	-	-
10x [TMA - $O_2^*$ ]	51.5	-	28.5	20	-	-
50x [TMA - $O_2^*$ ]	61	-	5	34	-	-
100x [TMA - $O_2^*$ ]	49	-	28	23	-	-

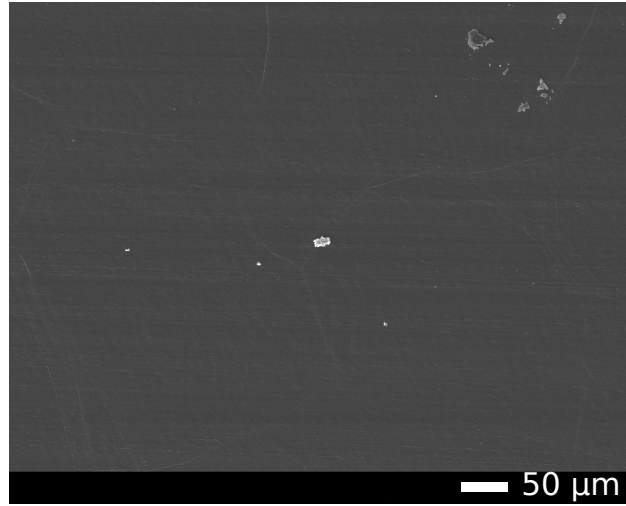


Figure S9: SEM image of 100 cycles TMA- $O_2^*$  on a  $O_2^*$  pretreated lithium foil.

Initially, more material is incorporated and growth on  $O_2^*$  -treated lithium is expected to be higher. However, after 100 cycles of TMA -  $O_2^*$ , the Al  $K\alpha$  signal detected by EDX falls between that of 100 and 200 cycles of TMA -  $O_2^*$  on Si, indicating ALD-like growth behavior.

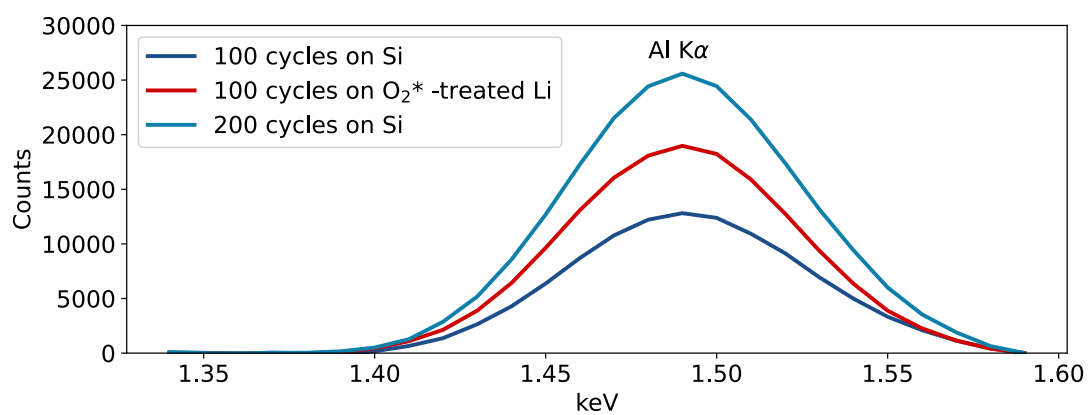


Figure S10: Comparison of the Al K $\alpha$  peak, measured by EDX, for 100 cycles of TMA - O<sub>2</sub>\* on O<sub>2</sub>\* treated Li and on Si.

## Importance of the LiOH component

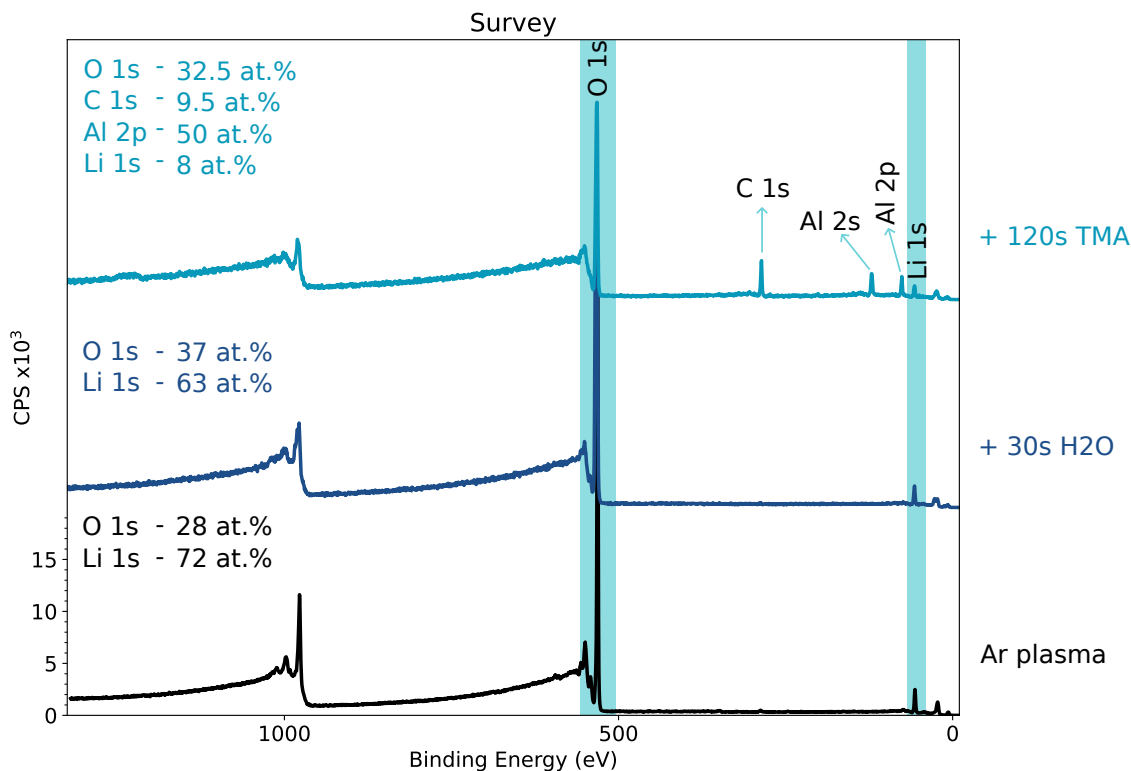


Figure S11: XPS survey scans of an Ar plasma treated lithium foil exposed to 30s of  $\text{H}_2\text{O}$ , followed by a 120s TMA exposure.

Additional hydroxylation experiments were performed to estimate the LiOH fraction required at the surface to obtain ALD-like behavior.  $\text{Ar}^*$  treated foil was exposed to brief  $\text{H}_2\text{O}$  doses, 2 and 5s at  $10^{-3}$  mbar, each resulting in a LiOH: $\text{Li}_2\text{O}$  fraction of approximately 30:70 derived from O 1s peak fitting, as shown in Figure S12. Similarly, leaving an  $\text{Ar}^*$  treated foil in UHV overnight led to the formation of a mixed LiOH/ $\text{Li}_2\text{O}$  surface with a comparable ratio of 30:70. For all of these surfaces, subsequent TMA exposure showed self-limiting behavior. These observations indicate that the LiOH: $\text{Li}_2\text{O}$  ratio of 30:70 at the surface is already sufficient to obtain ALD-like behavior and suppress TMA decomposition. However, since lower LiOH fractions could not be achieved, this value should be regarded as an approximate lower bound.

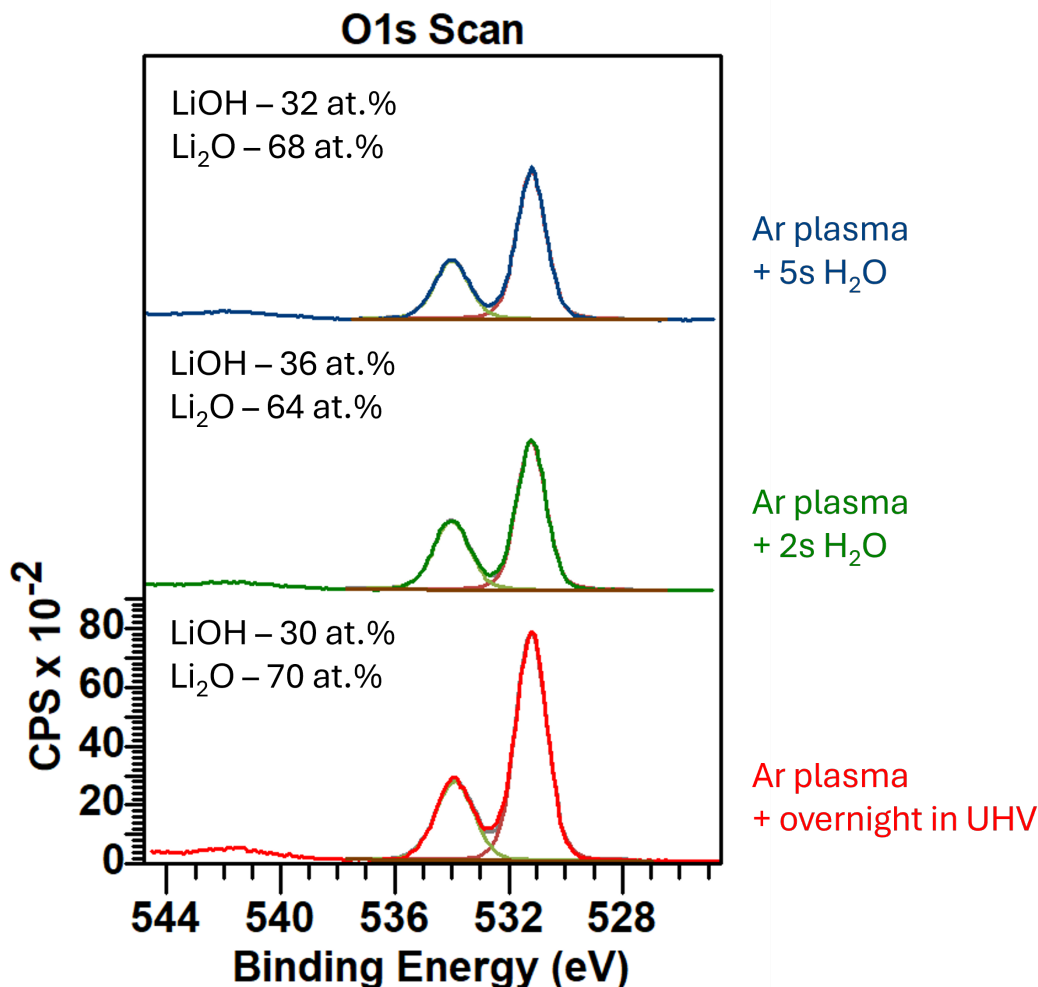


Figure S12: XPS O 1s high-resolution spectra of Ar\* treated lithium foils after ‘controlled’ hydroxylation through (red) overnight exposure in XPS UHV and brief H<sub>2</sub>O doses of (green) 2s and (blue) 5s.

Although a LiOH component can also be obtained by dosing an Ar\*-treated surface with H<sub>2</sub>O, this approach is not suitable for ALD. The reaction between H<sub>2</sub>O and metallic lithium is not self-limiting, but instead proceeds continuously, with the thickness of the LiOH layer increasing with exposure time (Figure S13).<sup>2</sup> Consequently, a thermal TMA-H<sub>2</sub>O process is unlikely to exhibit ALD-like behavior on a metallic lithium surface, which may complicate precise growth control and reproducibility.<sup>3</sup>

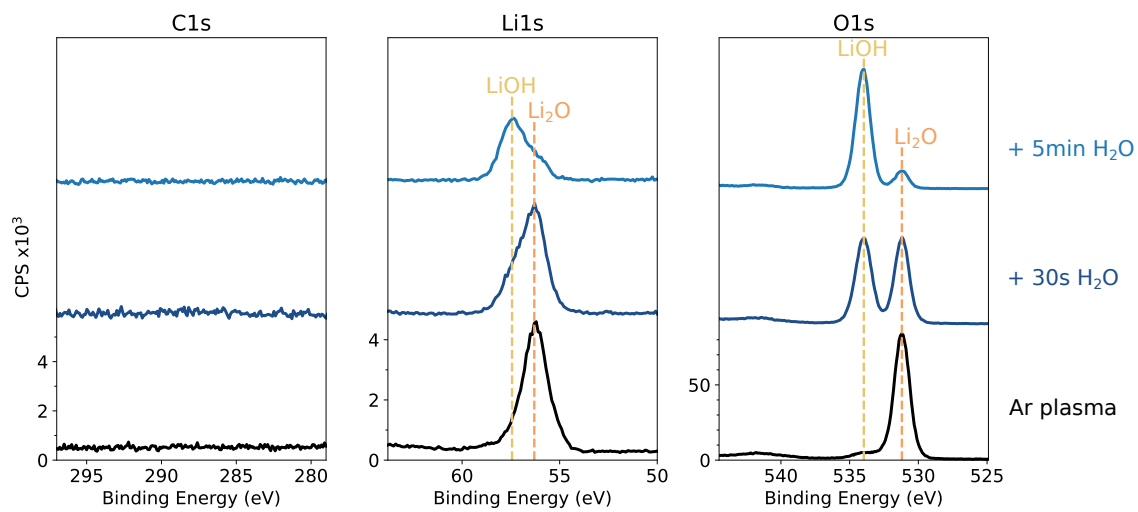


Figure S13: XPS high-resolution scans of different H<sub>2</sub>O dosing times on an Ar\*-treated lithium surface.

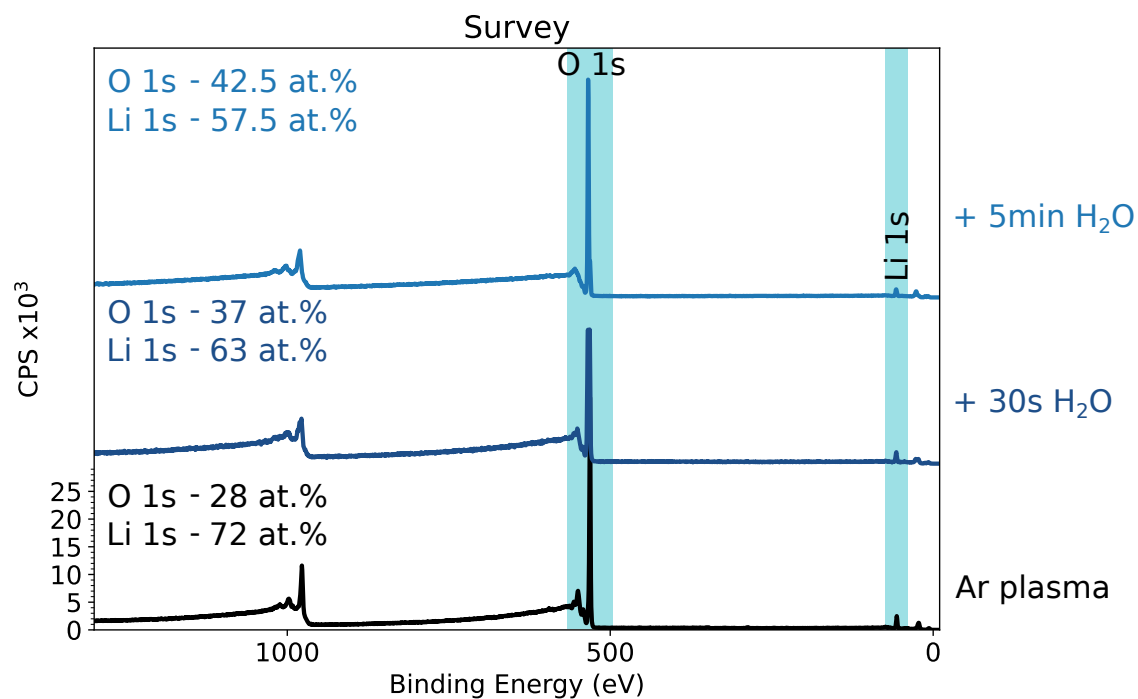


Figure S14: XPS survey scans of different H<sub>2</sub>O dosing times on an Ar\*-treated lithium surface.

## Pilling-Bedworth Ratio

The Pilling-Bedworth ratio (PBR) is the ratio of the molar volume of the metal oxide and the molar volume of the corresponding metal, as described in Equation 1.<sup>4</sup> Based on this ratio, it can be judged whether the oxide can completely cover and protect the metal on which it forms.

$$R_{PB} = \frac{V_{oxide}}{n \cdot V_{metal}} = \frac{M_{oxide} \cdot \rho_{metal}}{n \cdot M_{metal} \cdot \rho_{oxide}}, \quad (1)$$

with  $V_x$  the molar volume of x, n the number of metal atoms in the chemical formula of the oxide,  $M_x$  the molar mass of x and  $\rho_x$  the density of x.

If the  $PBR < 1$ , the oxide volume is smaller than the metal volume. The formed oxide layer will be porous/cracked and is not able to protect the underlying metal from further oxidation.

On the other hand, a ratio larger than 2 is caused by an oxide volume significantly larger than the metal volume. The compressive stress will result in cracking of the oxide layer and the oxide will flake off, also leaving the metal unprotected.

When the ratio lies between 1 and 2, the molar volumes are more comparable. This results in a formed oxide layer which completely covers the underlying metal.

The calculated PBRs in Table 2 shows that the PBR for  $Li_2O$  is smaller than 1, meaning the oxide layer is likely to be porous and therefore the underlying metallic lithium is still exposed, while  $LiOH$  and  $Li_2CO_3$  can passivate the surface.<sup>2</sup>

Table 2: Pilling-Bedworth ratio for different lithium compounds typically formed on metallic lithium.  
 $M_{lithium} = 6.941$  g/mol,  $\rho = 0.534$  g/cm<sup>3</sup>

	Li <sub>2</sub> O	LiOH	Li <sub>2</sub> CO <sub>3</sub>
$M_{oxide}$ (g/mol)	29.882	23.949	73.892
$\rho_{oxide}$ (g/cm <sup>3</sup> )	2.01	1.46	2.11
PBR	0.57	1.26	1.35

## References

- (1) Werbrouck, A.; Van de Kerckhove, K.; Depla, D.; Poelman, D.; Smet, P. F.; Dendooven, J.; Detavernier, C. Plasma-enhanced atomic layer deposition: Correlating O<sub>2</sub> plasma parameters and species to blister formation and conformal film growth. *Journal of Vacuum Science & Technology A* **2021**, *39*, 062402.
- (2) Otto, S.-K.; Fuchs, T.; Moryson, Y.; Lerch, C.; Mogwitz, B.; Sann, J.; Janek, J.; Henss, A. Storage of Lithium Metal: The Role of the Native Passivation Layer for the Anode Interface Resistance in Solid State Batteries. *ACS Applied Energy Materials* **2021**, *4*, 12798–12807.
- (3) Chen, L.; Connell, J. G.; Nie, A.; Huang, Z.; Zavadil, K. R.; Klavetter, K. C.; Yuan, Y.; Sharifi-Asl, S.; Shahbazian-Yassar, R.; Libera, J. A.; Mane, A. U.; Elam, J. W. Lithium metal protected by atomic layer deposition metal oxide for high performance anodes. *J. Mater. Chem. A* **2017**, *5*, 12297–12309.
- (4) Xu, C.; Gao, W. Pilling-Bedworth ratio for oxidation of alloys. *Material Research Innovations* **2000**, *3*, 231–235.